CHALMERS

On-line Capacitive Moisture Measurement of Iron Ore Concentrate

Construction of an on-line, contactless, prototype sensing system for industrial applications

Bachelor's Thesis at the Department of Electrical Engineering

Kevin Bäckstäde, Pontus Liljeberg, Måns Lundberg, Ramazan Murtazaliev, Nils Wastegård, Axel Widlund

DEPARTMENT OF ELECTRICAL ENGINEERING
CHALMERS UNIVERSITY OF TECHNOLOGY
Gothenburg, Sweden 2025
www.chalmers.se

Bachelor's thesis 2025

On-line Capacitive Moisture Measurement of Iron Ore Concentrate

Construction of an on-line, contactless, prototype sensing system for industrial applications

Kevin Bäckstäde
Måns Lundberg
Pontus Liljeberg
Ramazan Murtazaliev
Nils Wastegård
Axel Widlund

CHALMERS

Department of Electrical Engineering
Chalmers University of Technology
Gothenburg, Sweden 2025

On-line Capacitive Moisture Measurement of Iron Ore Concentrate.

KEVIN BÄCKSTÄDE
PONTUS LILJEBERG
MÅNS LUNDBERG
RAMAZAN MURTAZALIEV
NILS WASTEGÅRD
AXEL WIDLUND

Supervisor: Viktor Lindström, Systems and Control, Electrical Engineering
Examiner: Torsten Wik, Systems and Control, Electrical Engineering

Bachelor's Thesis 2025
Department of Electrical Engineering
Division of Systems and Control
Chalmers University of Technology
SE-412 96 Gothenburg
Telephone +46 31 772 1000

Cover: Picture of small-scale rotating conveyor with iron ore concentrate
Typeset in LaTeX
Printed by Chalmers Reproservice
Gothenburg, Sweden 2025

Abstract

Accurate moisture determination of iron ore concentrate, also referred to as ore concentrate, is important to the production of iron ore pellets. Existing methods have long response times, sampling variability and/or require manual work. Capacitive methods for moisture determination show promising signs of solving several of these problems.

To determine the feasibility of constructing an on-line measurement sensor utilising capacitive methods, a small-scale prototype consisting of a rotary conveyor dish, a capacitive sensor and measurement electronics was constructed. The sensor consists of two pairs of electrodes, each of which constitutes a capacitor with the surrounding material as dielectric. By placing the sensor below the rotational dish, allowing the measured iron ore concentrate to compose most of the dielectric medium, its permittivity, which will vary with its moisture content, can be measured as a change in capacitance.

Testing was performed to determine the effects of varying frequency, mass and speed of the measured material. The results show that even though there seems to be a strong correlation between the measured capacitance and the moisture content, it is hard to draw any direct conclusions on the correlation due to high local variability in the material, leading to uneven sampling and poor verification tests. Further tests on a larger scale are suggested to remedy these problems.

Keywords: capacitance, contactless, iron ore concentrate, iron ore moisture, LKAB, moisture content, on-line, resonance

Acknowledgements

This project would not have been possible without the help and support of several people. Firstly, we want to thank our supervisor Viktor Lindström for his guiding expertise, providing us with equipment and designs, and our examiner Professor Torsten Wik for his patience and guiding words. Further, we want to thank Lars Pettersson, who contributed to the proposal of this project, and John-Erik Rutström at LKAB for their support and help. Without the support and guiding expertise of Rikard Karlsson and Douglas Jutsell Nilsson, both lab managers of the CASE-lab at Chalmers, who provided us with laboratory premises, this project would not have been able to leave the theoretical stage. Lastly, we want to thank our fellow students and friends for acting as a sounding board and elevating this report to a higher standard.

Kevin Bäckstäde, Pontus Liljeberg, Måns Lundberg,
Ramazan Murtazaliev, Nils Wastegård and Axel Widlund
Gothenburg, May 2025

Glossary

Agglomeration	Process where particles lump together to form larger particles. In this case, the formation of raw iron ore pellets.
Attenuation	Reduction in the amplitude of a signal.
Blast furnace	Smelting furnace in the shape of a tower where ore is processed into iron with the help of hot, compressed air, coke and other additives.
CDC	A device that converts capacitance measurements into digital signals, commonly used in different sensing applications.
Chalmers	Chalmers University of Technology, Technological university located in Gothenburg, Sweden.
Concentrate	Fine-grained ore where the concentration of the metal has been increased.
Dielectric medium	An insulating, or poorly conducting material that can support electrostatic fields.
Direct reduction plant	Process where iron ore is reduced to iron without melting.
Filtrate water	Water which has passed through a filter, in this case water removed from a slurry.
FMEA	A systematic method for identifying potential failure modes in a system.
LC-tank	An electric circuit consisting of a capacitor and an inductor, which can be used as a resonator, oscillating at a certain frequency decided by its size.
LKAB	Lousavaara Kirunavaara Aktiebolag, Swedish state-owned mining and refining company.
Lot	Discrete and defined quantity of a material.
On-line measurement	Measurements performed automatically.
Pellet	A small, rounded, compressed mass of a substance.

Permittivity	The relative permittivity (ε_r) is a unit-less measurement of how much of a material can be polarized in an electric field.
PID controller	Proportional-Integral-Derivative controller. A feedback control system used to maintain a desired output. It combines proportional (present error), integral (accumulated past error), and derivative (predicted future error) to achieve a stable output.
Printed Circuit Board	A sheet of layered silicone and etched copper paths designed to connect multiple electronic components into a larger system.
R^2 **value**	The variance in the dependent variable that is explained by the independent variable in a regression model, with values closer to 1 indicating a better fit.
Rotary optical encoder	A rotary encoder that uses light to detect position and rotation.
Sintering	Process of turning a loose material into a solid with the help of heat below the material's melting temperature.
Slurry	A mixture of denser solids suspended in liquid, usually water, in this text referring to iron ore suspended in water.

Contents

List of Figures

List of Tables

1
Introduction

1.1 Background

In modern steel production, it is common to use iron ore pellets to improve transportability, the chemical composition and process efficiency. Turning raw iron ore into pellets is a multi-step process where mined ore is crushed, sorted, concentrated and purified. This process is partly aided by water, which results in a slurry consisting of finely ground iron ore and water. In order to form raw pellets, the slurry is dewatered or filtered, resulting in a concentrate which is then agglomerated into balls, raw iron pellets, in rotating dishes or drums. The raw iron pellets are then dried, preheated, and sintered into finished pellets which can be used in both blast furnaces and direct reduction plants. The largest iron ore producer in Europe, Swedish Lousavaara Kirunavaara Aktiebolag (LKAB), relies on this process for most of its production, which is predominantly shipped within Europe, but also to the rest of the world, where it can be processed into steel.

The moisture content of the iron ore concentrate is essential in ensuring the correct conditions for agglomeration to form the raw pellets [1], [2]. If the concentrate is too wet, it may not be able to hold the shape of a ball, and if it is too dry, it may fail to agglomerate at all. Further, the energy-intensive process of drying and sintering the pellet emphasises the need to accurately measure the moisture content. A higher water content would lead to higher energy consumption, since more water needs to evaporate when drying the pellets. As discussed further in Section 1.5, the conventional methods of determining moisture content typically have long response times. This causes a delay in the regulation of the moisture filtration process. Improvements to this method could potentially increase the throughput and energy efficiency of the filtering process by reducing the variability of the moisture content in the concentrate.

1.2 Problem Definition

This project aims to answer the following main questions:

- What is the feasibility of implementing capacitive iron ore concentrate moisture content measurement in real-time?
- How does the capacitive moisture measurement system compare to traditional methods?

These questions will be answered and evaluated by focusing on three main areas: the design, the measurement signal and the evaluation method of the sensor.

1.3 Delimitations

To limit the scope of the project, three main delimitations were set. The main goal of these delimitations was to enable testing in existing facilities without complicated logistics.

This project only focused on one concentrate product quality, which was chosen after consultation with LKAB. The reasons for this were several. For example, the additives in the concentrate change with product quality. By limiting the work to the same product quality, focus can be placed on examining moisture content. The choice of product quality also ensured access to concentrate throughout the project. The nominal moisture of the concentrate is 9 % with an assumed possible variation of ±3 %.

To enable tests without the need for a climate-controlled environment, this project does not include measurements of surrounding temperature and humidity in any calculations. Instead, they were recorded and will be discussed in the error analysis.

No connection to the control system of the processing plant was considered.

1.4 Conflict of Interests

This project was performed in cooperation with the mining company LKAB, which provided materials for testing as well as financed some of the electronics used. They also provided consultation on subject matters. One of the project members previously worked at LKAB with the pelletisation process and is currently employed by LKAB but with no direct involvement in subjects of this project. LKAB has not exercised any influence on the scientific process of this project, neither economic nor by other incentives.

1.5 Existing Methods

Several methods to determine the moisture content of iron ore concentrate and other materials are already well established in the industry today. The most relevant for this project will be discussed below.

1.5.1 Gravimetric Methods

One of the more common methods used to determine the moisture content of a bulk material is the loss-on-drying method, which is the method used in LKAB:s processing plants today. The method involves taking a sample and drying it until no

more weight is lost. The moisture content can be calculated by subtracting the dry weight from the initial weight. This method takes several hours to return a result, but is very accurate [3]. It is also difficult to implement as an on-line measurement [4], leading to introduced sampling variability and lower accuracy [5]. The drying can be performed in an oven or a special moisture-content scale with built-in drying methods.

1.5.2 Microwave Methods

There are two main methods based on microwave radiation, one uses phase shift and the other uses attenuation to determine the moisture content. When a microwave beam travels through water, a phase shift is caused. This phase shift is typically much larger in water than the material in which the water is entrained. By sending a beam of microwaves through a bulk material and measuring the phase shift, it is possible to infer a correlation between its moisture content and the phase shift, making it usable in continuous measurement applications like conveyor belts. However, using the method for iron ore concentrate has proved challenging mainly due to the high attenuation of the signal [6].

The other method, using attenuation, works by analysing how much a signal is attenuated when passing through a material and, by measuring this, determining the water content. The attenuation and phase shift methods are both considered high investment and are sensitive to the surrounding environment, such as metal in the signal path [4].

1.5.3 Optical Methods

When light is reflected off a material, the absorption depends on the light's wavelength. Through choosing wavelengths for which water has specific characteristics, it is possible to determine the moisture content by analysing the reflected light. This method has been successfully tested in the industry with a deviation of $\pm 0.3\,\%$ [7].

Later tests have shown non-trivial calibration problems, significant variations in variability from varying production, and no better accuracy than current methods. However, the improved sampling rate and response time have been highlighted as advantages. The method also requires some mixing of the iron ore concentrate before the measurement point, since it will only measure on the exposed top layer [5].

1.5.4 Capacitive Methods

Capacitive methods present an alternative approach to moisture measurement that relies on the principle that the permittivity, or dielectric constant, of a porous material changes significantly with its water content. A capacitive sensor essentially forms a capacitor where the measured material acts as the dielectric medium between two or more electrodes. The capacitance of this arrangement is directly influenced by the permittivity of the material. As the moisture content within the iron ore

concentrate increases, the overall permittivity of the material also increases because water has a much higher permittivity than air and the dry iron ore components [8]. Consequently, this change in permittivity leads to a measurable change in the capacitance of the sensor. By establishing a relationship between the measured capacitance and the moisture content through calibration, this method can be used for moisture determination. Capacitive sensors are commonly employed in applications such as soil moisture measurement and liquid level sensing due to their relatively simple design, robustness, and potential for cost-effective implementation [9]. Research in Brazil [10] has demonstrated the feasibility of using capacitive methods for measuring moisture content in iron ore concentrate, suggesting its potential as a viable alternative to traditional techniques.

1.6 Scope

Given the limited research into using capacitive methods for iron ore concentrate, which shows promising signs of being feasible compared to the other methods, the purpose of this project has been to explore the feasibility of employing capacitive sensing technology for real-time moisture measurement, specifically in iron ore concentrate. By undertaking the design, construction, and testing of a prototype sensor system, this research aims to determine whether this method can provide reliable and accurate moisture content data that is responsive enough for real-time process control. The successful implementation of such a system could offer significant advantages over existing methods, potentially leading to improved process control and enhanced energy efficiency in the iron ore pelletisation process. The focus will be on evaluating the sensor's performance under conditions relevant to the industrial environment, considering factors such as the material's movement, varying moisture content, and potential environmental influences.

2

Methodology and Theoretical Framework

This chapter describes the methodology applied during the measurements and the theoretical concepts that support it. Given the novel character of the project, the method and theory are integrated to provide a unified and comprehensive overview.

2.1 Theoretical Basis

The method of measuring the moisture content of a bulk material with the help of capacitance, as introduced earlier, relies on the following physical principles.

2.1.1 Basics of Capacitors

A capacitor is a simple electric component that can store electrical energy as an electrical potential. When two conductors containing movable electric charges are placed with an isolator or dielectric separating them, and an electric potential is applied over them, electrons travel from one side to the other. Electrical energy is thereby stored in the capacitor. The magnitude of the charge is proportional to the potential difference of the two conductors

$$Q = C\Delta V \tag{1}$$

where Q is the charge in C, C is the capacitance in F and ΔV is the difference in voltage over the two conductors in V. When conductive surfaces are involved, capacitance is related to the area of those surfaces, their distance from each other, and the relative permittivity of the dielectric separating them

$$C = \varepsilon_0 \varepsilon_r \frac{A}{d} \tag{2}$$

where C, as above, is capacitance, ε_0 is the permittivity of vacuum, ε_r is the relative permittivity of the dielectric medium between the conductive surfaces, A is the area in m^2 and d is the thickness of the dielectric in m [11].

2.1.2 Dielectrics and Permittivity

A dielectric material is typically an insulator that can be polarised by an electric field, although most materials display dielectric properties. The relative permittivity of a dielectric, ε_r, denotes the material's ability to support an electric field.

The permittivity of a material is not fixed but varies slightly with parameters like frequency of the electrical field, temperature and humidity [11]. The relative permittivity of air is approximately 1, while that of water is around 80, which makes it possible to determine the content of water in a bulk material by analysing its relative permittivity. This can be done by constructing a capacitor where the dielectric is made up of that bulk material [12].

2.1.3 Resonator Circuits

A circuit consisting of a capacitor and an inductor in parallel, also known as a LC-tank, has a natural resonance frequency determined by:

$$f_{resonance} = \frac{1}{\sqrt{LC}} \tag{3}$$

Where L is the circuit's inductance in H and C is the capacitance in F. This relation stems from the nature of how charges are alternating between being stored in the capacitor and the inductor. By measuring the resonance frequency and knowing either one of the circuit's capacitance or inductance, the other parameter can be deduced [13].

2.2 Sensor Construction

The sensor in its entirety consists of a few different, interconnected parts, illustrated in Figure 1.

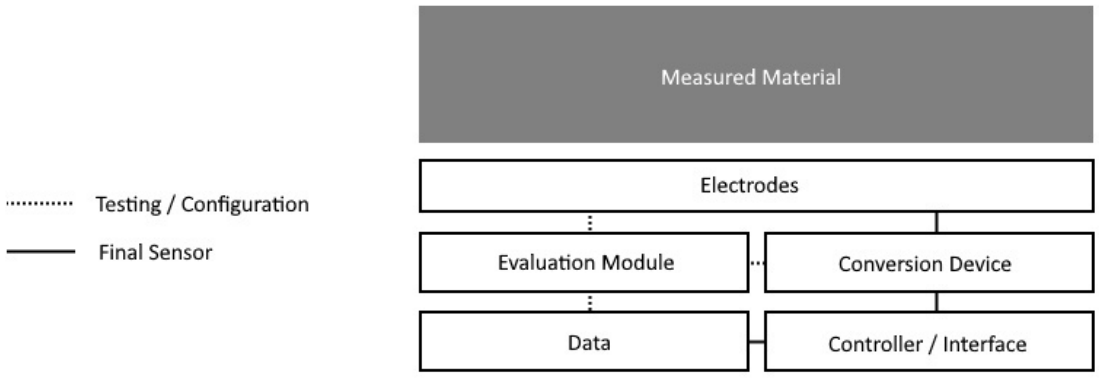

Figure 1: Sensor-System Overview Diagram

- **Electrodes** - Conductive plates placed near the iron ore concentrate, subject to electromagnetic effects of the nearby environment, including said material's dielectric properties and proximity.

- **Conversion Device** - Method for converting electromagnetic effects experienced on the electrodes into a numerically quantifiable property.

- **Controller And Interface** - Device configuring the conversion device to be in the correct state, handles the logic of reading and potentially transforming conversion results and sending them to where they need to be.

- **Evaluation Module** - A pre-assembled development board with verified functionality, useful for configuring and verifying the function of a custom conversion device.

- **Data** - Generated stream of data that can be analysed on-line in real-time or stored for later off-line analysis.

2.2.1 Electrodes Construction

Two electrodes were made from copper tape applied to acrylic blocks and aligned in a coplanar configuration. This was done to promote electric fields that extend outward radially and enable contactless measurements at a distance. Shielding planes were formed with additional copper tape opposite to the electrode signal plane and on the sides of the acrylic block for each respective electrode, creating a controlled area resistant to electromagnetic noise and capacitive objects in the direction blocked by the shield [14]. An illustration of an electrode pair is available in Figure 2.

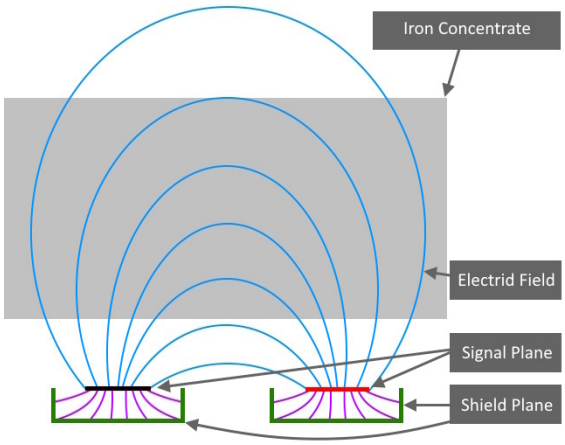

Figure 2: Illustration of electrodes cross-section

The electrodes were each soldered to coaxial cables inserted through a hole in the shield plane, and the shield plane was soldered to the braided shielding of that same coaxial cable. The cables were subsequently fitted with SMA connectors on the opposite ends to make them easy to connect and disconnect as needed.

The area of the electrode signal planes is a property that should be maximised to be sensitive to changes in the dielectric properties of the measured material, as follows from Equation 1. The length of the electrode, however, is constrained by the sensing geometry of interest, since electrodes that extend beyond that area would only introduce more undesired environmental variation with little or no increase in

sensitivity. For this study, a rotary conveyor, described in Section 2.4, was constructed as a platform to perform the tests on. A conveyor width of 185 mm was decided, and for some extra margin to the conductive steel ring edges, an electrode length of 120 mm was deemed suitable.

The separation of the electrodes can be thought of in terms of the desired measuring depth. The further the electrodes are from each other, the weaker the electric field gets. But, with a larger separation, a higher proportion of the sensed signal comes from within the material. This is demonstrated geometrically in Figure 3.

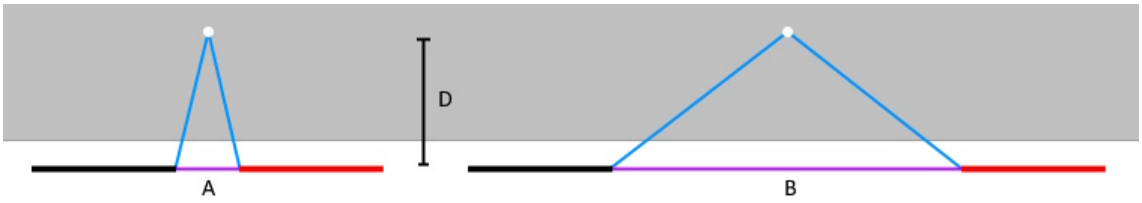

Figure 3: Illustration of electrodes separation

Comparing the direct paths A and B with their respective paths going through a point at depth D in the sensing area, we can see that the path going through the material gets more and more equidistant to the direct path the further apart the electrodes are. The interactions of electric fields with porous and slightly conductive materials like iron ore concentrate, however, are very complex. For this reason, the electrode separation was left adjustable to be tinkered with further. In the end, separations of 23 mm and 35 mm were used on two separate channels for all tests.

The electrode width was set in relation to the electrode separation according to a ratio

$$T = 1.35g + 0.65s \tag{4}$$

discovered in a previous study [10], where T is signal depth, g is half the separation and s is electrode width. Copper tape easily available for this study was 19 mm wide. For a separation of around 30 mm this would correspond to a signal depth of 32.6 mm, which is reasonable.

Finally, the distance from the shield to the electrode signal plane is a property sought to be maximised in order to minimise parasitic capacitances. The thickest, easily available acrylic during this study was 8 mm thick, which is a significant shield distance, and as such ended up being the distance that was realised in the final design. A render and a drawing of this design are found in Figures 4 and 5.

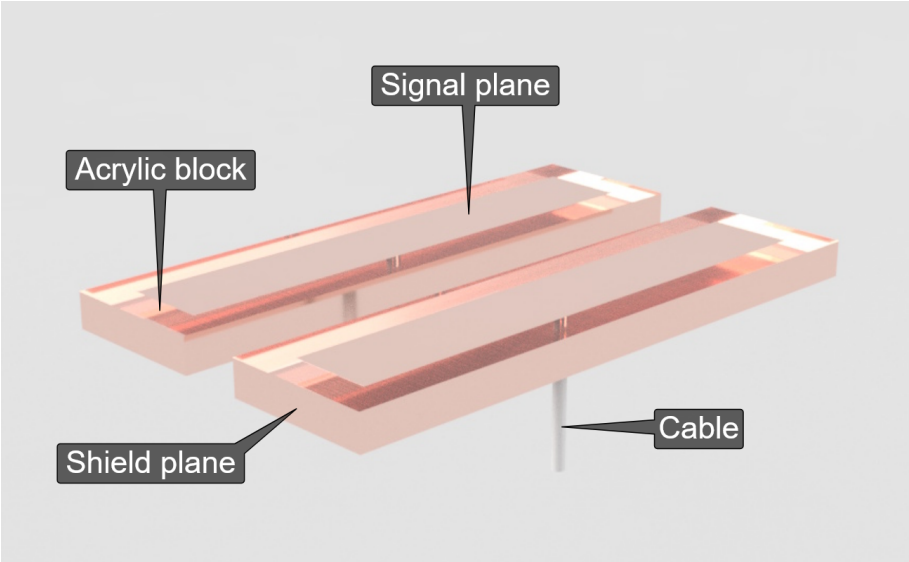

Figure 4: Render of electrodes

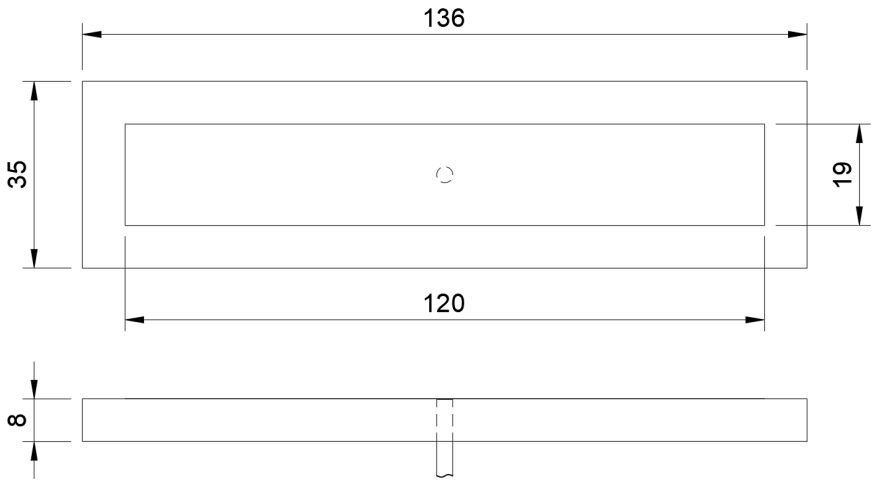

Figure 5: Drawing of an electrode

2.2.2 Conversion Device Construction

As capacitance-digital-converter (CDC), FDC2214 was selected as the conversion device of choice for its highly accurate, resonance circuit conversion method, enabling resolution of as good as 0.4 fF [15]. However, the FDC2214 outputs neither a resonance frequency nor a capacitance directly; rather, a lower-level property referred to as raw code that comes from counting the number of resonance signal peaks during a fixed number of crystal oscillator cycles. With a known oscillator frequency and known LC-tank properties, however, both resonance frequency ($f_{SENSORx}$) and capacitance ($C_{SENSORx}$) can be calculated as

$$f_{SENSORx} = \frac{f_{REF} \cdot DATAx \cdot CHx\_FIN\_SEL}{CHx\_FREF\_DIVIDER \cdot 2^{28}} \tag{5}$$

$$C_{SENSORx} = \frac{1}{2\pi(L_x \cdot f_{SENSORx})^2} - C_x \tag{6}$$

with parameters as below:

f_{REF} - Crystal oscillator reference frequency
$DATAx$ - Raw code Conversion result from channel x
CHx_FIN_SEL - Input frequency select setting on channel x
$CHx\_FREF\_DIVIDER$ - Reference frequency divider on channel x
L_x - Fixed LC-tank inductance on channel x
C_x - Fixed LC-tank capacitance on channel x

according to the datasheet of the FDC2214 [15].

A custom PCB developed in a previous work by Viktor Lindström at Chalmers university of technology (CTH) was utilised for the implementation of the FDC2214. This was done because the design provided extensive configurability, such as swappable LC-tanks, integrated passive shielding, and cable connectors, as well as to save time and to expedite initial results.

The FDC2214 was configured according to the instructions in the datasheet and tweaked to output highly accurate values in exchange for a slower output rate [15]. For the operating conditions described above, the configuration deemed most suitable for tests can be found in Appendix A.

2.2.3 Controller And Interface Construction

An Arduino MKR Zero was used to control and communicate with the conversion device as well as to provide a user interface for operators. The MKR-Zero is a flexible development board with an inbuilt SD-card reader, which is desired for the system to be able to store data independently, as mentioned in Section 1.2. The interface in the case of this study consisted of buttons for starting and stopping the logging of data, together with some LED diodes and an OLED display to communicate the state and status of the sensor system.

2.2.4 Data Logging

A simple protocol for log files with raw code output data of the FDC2214 was developed and contains two parts: One section for constant data in JSON format used to save information such as which LC-tank was used, and another section for a

chronological stream of output data with timestamps. With the help of the raw code conversion formulas in Equations 5 and 6, the log data could later be transformed into the preferred format and plotted and analysed in any way necessary.

2.2.5 Evaluation Module Usage

The Texas Instruments evaluation module and Sensing Solution software suite were used to ensure the electrodes were functioning well and to verify that changes in the environment, such as the proximity of a hand or conductor, could be detected at a very early stage of development. They also served the purpose of finding the right configuration for a given LC-tank since the software's graphical user interface provided detailed and comprehensive guidance about any out-of-spec values.

2.3 Iron Ore Concentrate

Table 1: Selected moisture contents to test feasibility of measurement precision of 0.03 %, calculation is presented in appendix F

Sample Nr.	**Moisture Content (%)**
1	6.00
2	8.19
3	8.78
4	8.94
5	9.00
6	9.03
7	9.11
8	9.41
9	10.55
10	12.00

Sampled iron ore concentrate was delivered by LKAB in 15 containers, see Figure 6 weighing approximately a total of 150 kg to ensure sufficient material for multiple tests. This sampled concentrate is what the project used to test the measuring method and equipment, and its moisture content was decided with the gravimetric method described in 2.3.1. Out of the 15 lots, 10 were designated moisture contents, which lay in the entire testing area according to Table 1. The five remaining lots were left at approximately 8.7 % to be used in tests that required more material.

Figure 6: Container with iron ore concentrate sampled from LKAB processing plant

By designating moisture contents to different lots and keeping the lots in sealed containers, the need for adjusting moisture is reduced, thus minimising the need for wetting and drying the concentrate. However, since all lots are sampled from the production line, their initial moisture content needs to be adjusted. To ensure representative contents of minerals, filtrate water from the production facility was used to wet concentrate that needed increased moisture content, while concentrate with a lower desired moisture content were either air dried outside their airtight containers or partly dried in an oven and then mixed. The remaining five lots can be used in tests where the effects of movement need to be studied.

2.3.1 Moisture Verification

This section describes the method used to verify the moisture content of the materials tested. It is derived from the gravimetric method described in ISO 3087:2011 [3].

To ensure a representative sample for the process, the whole lot is first homogenised as described in the next section. Given the importance of accurate weight measurements, a scale with high precision was chosen. The scale, Kern EHA 500-2 with a precision of 0.01 g, has a maximum weighing capacity of 500 g [16]. To ensure a precision of at least 0.01 %, a sample of no less than 100 g of concentrate was added to a pre-weighed, oven-safe beaker as seen in Figure 7. In accordance with the specifications of the ISO standard, the material was then dried for four hours and weighed again, allowing the lost water to be calculated and thus the initial moisture content. The standard states that samples over 8 % should be dried for no less than 24 hours, but two tests were performed where the moisture content of 12 % was determined to be dry after only four hours through weighing after one additional hour and determining that the mass was not dropping further. This deviation, to only dry in the oven for four hours, was determined to be minuscule and not affect

Figure 7: Four samples during drying in oven

the measurements.

To reduce waste of material, the dried samples were put back with the original lot in the containers and the lost mass was readded as deionised water to introduce as few minerals and other materials as possible which could affect measurements.

2.3.2 Sample Quality Assurance

To verify the moisture content, a gravimetric analysis (SS-ISO 3087:2011 [3]) was conducted on subsamples using a POL-EKO SLW 75 smart oven and a Kern EHA 500-2 scale. However, deviation from the ISO-standard was made due to the limited lot sizes; according to the standard, it should be at least 1 kg, whereas for these tests, the subsamples were 100 g, as mentioned earlier. Another deviation from the ISO standard was that only one sample was taken from each lot instead of four samples, as in the standard. This was due to the limited lot sizes. The gravimetric analysis was used to verify the lot moisture and be able to set them according to Table 1, but also once for each sample for each test to account for evaporated water between tests.

A custom mixer tool was made to homogenise the tests, see Figure 8. This was after realising the concentrate behaves unexpectedly and creates lumps with higher moisture content than the rest of the sample.

When weighing the whole sample in the container, we used a Kern DE 60K10D, however, it has an error margin of 10 g, which resulted in some trouble when wetting the material to the predetermined moisture contents [17]. This made the gravimetric method test even more vital to ensure that our samples were correct.

A source of error to take into consideration is the nugget-to-sill ratio. The nugget effect is a phenomenon that shows when small randomised differences occur in a small sample, while the sill describes the total variability in the sample. The Nugget-to-Sill ratio is the effect of the nugget divided by the effect of the sill. This gives a perception of how homogenised a sample is [5].

Figure 8: The device designed for mixing, crushing and homogenising iron ore concentrate

2.4 Rotary Conveyor

A test rig for the sensor prototype in the form of a rotary conveyor was constructed to simulate the conveyor belt in the plant on a small scale. To allow for consistent tests with movement, it is constructed as a rotary dish so that the samples stay the same each time they pass the sensor. This makes it possible to use the same samples multiple times while testing different parameters.

2.4.1 Rotary Dish

The dish is made out of 3 mm thick acrylic supported by 2 mm thick steel rings on either side. Acrylic was chosen as an alternative to rubber because it has little impact on capacitive measurements and can easily be cut to shape using a laser cutter while also being stiff enough to support the weight of the ore without bending much. If the band bends, the distance to the sensor could vary, introducing a source of error in measurements.

At the plant, the conveyor is 2400 mm wide and 15 mm thick. The test rig has a scale of 1:13, limited by the acrylic sheet width available to the project, making the test surface 185 mm wide. Unfortunately, it was not possible to match the scale for the thickness of the belt as it became too unstable with thinner material than 3 mm. A drawing of the dish can be seen in Figure 9.

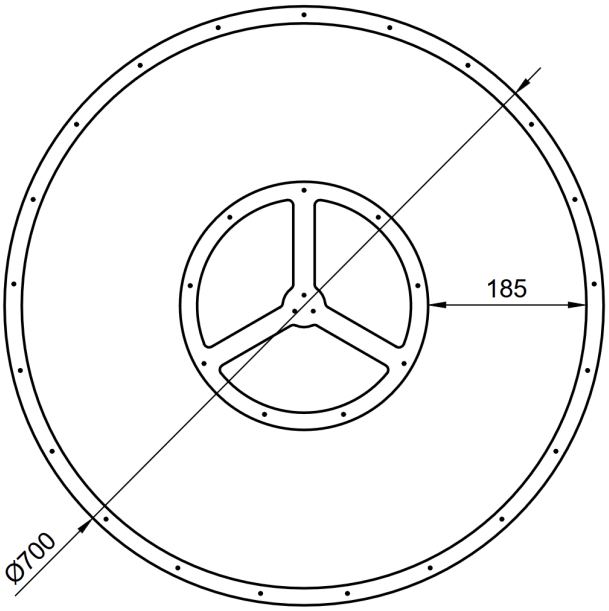

Figure 9: Conveyor Dish Drawing

2.4.2 Frame and Sensor Mount

The dish rests on four ball bearings supported by a structure made from 2 mm thick steel parts held together by nylon brackets that were 3D-printed. This structure has adjustable feet to make it level. The sensors are also attached to this structure with an adjustable holder made from PLA plastic, which allows for adjustments both vertically to tune the distance from the acrylic and horizontally to tune the distance between the sensor plates. A drawing of this mount can be seen in Appendix B. All the electronics supporting the sensors and data logging are mounted in a box below them. The sensor configuration and supporting electronics are described in Section 2.2.

2.4.3 Sample Partitioning

The circle is divided into eight sections, 45° each. These sections make it possible to run tests with eight different samples at the same time. For the initial tests, this was done by placing the concentrate in 3D-printed boxes made to fit the circle. The boxes were made to be able to easily move the samples into different configurations without having loose iron ore concentrate on the dish. These boxes were later abandoned as the distance to the sensor had a significant impact on the results, and there was uncertainty over whether the PLA plastic in the boxes would absorb too much moisture and cause errors in the results. Later tests were performed with 3D-printed walls that have slots for acrylic sheets to section off the different areas. This also allows for testing samples larger than 45°. These walls can be seen in Figure 10.

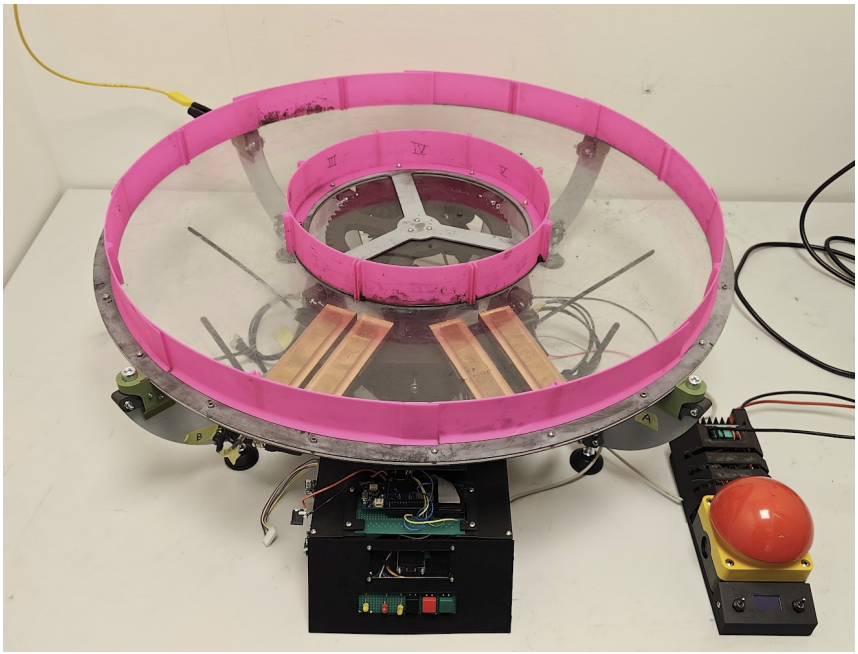

Figure 10: Picture of the test rig

2.4.4 Drive System

On the opposite side of the sensors, a DC motor with a 3D-printed gearbox that drives the rotation of the dish is mounted. The conveyor in the plant has a speed of $0.025\,\mathrm{m\,s^{-1}}$, which translates to 0.017 rps on the rig if the distance travelled is measured at the centre of the test area. At scale, this is 0.0013 rps. The gearbox has a reduction ratio of 750:1 to be able to reach this low speed. In the gearbox, there is also a rotary optical encoder used to find the current position of the dish as well as the speed. A drawing of this gearbox can be found in Appendix C.

A proportional-integral-derivative (PID) controller, together with the encoder readings, controls the rotation speed. The motor control electronics and interface are in a separate box connected to the rig. More information about the motor control

system can be found in Appendix D.

2.4.5 FMEA and Safety

A Failure Mode and Effects Analysis (FMEA) was conducted for both the sensor and the test rig to identify potential failure points that could compromise functionality or durability. This analysis guided the design phase to prevent future issues. The complete FMEA for the test rig is provided in Table 6 in Appendix E, while the sensor FMEA is detailed in Table 7 in Appendix E.

To ensure safety, protective barriers were installed to block access to hazardous areas, such as the gearbox and bearings. An emergency stop was implemented for the motor, and the motor driver circuit was connected to a current-limited power supply, always set below the motor's maximum rated current to avoid overloading.

2.5 Testing Methodology

The key goals of the following tests were to evaluate the sensor's sensitivity to its parameters and performance under controlled conditions, confirming expected behaviour and validating the equipment.

The chosen system, material, and environment variables that were tested are: LC-tank size, sample mass, sample compactness, sample speed during measurement, and lastly, iron ore concentrate moisture content.

2.5.1 Determination of Measurement Frequency

As mentioned in Section 2.1.2, the permittivity changes with the frequency of the electrical field applied. It was also hypothesised that different measurement frequencies would be affected differently by noise. To change the frequency of the capacitance-to-digital converter, the LC-tank size can be varied. To determine optimal frequencies, different sizes were tested to evaluate how the frequency affected the penetration depth as well as other complex frequency-dependent interactions, and therefore the measured output value.

Each test used three samples placed 120° apart on the rotating dish. Capacitance data was collected during 30 s intervals, alternating between measuring samples and the empty conveyor.

Samples with a dry weight of 946 g and moisture contents of 6.00 %, 9.00 %, and 12.00 %, were tested. These moisture contents were chosen to simplify the differentiation between samples. To prevent lumping, the lots were homogenised prior to sampling.

The measured parameters were the proportional variation in measurement during a selected interval and *sensitivity*, defined as

$$\text{Sensitivity} = \frac{\text{Value at } 12\% - \text{Value at } 6\%}{\text{Value at } 12\% - \text{Baseline}} \tag{7}$$

where the baseline is the measurement from the sensor with an empty conveyor. The sensitivity expresses the proportion between the range of interest and the full measured range. With higher sensitivity, as defined in Equation 7, the measurement range of the equipment is maximised for the data of interest.

To analyse the variation in the measured intervals, we need a way to describe how spread out the data is. Each measurement interval is indexed by i, which refers to a separate sample group in the test. A weighted mean, μ_w, is calculated using

$$\mu_w = \frac{\sum_i (\mu_i \cdot n_i)}{\sum_i n_i} \tag{8}$$

where μ_i is the average capacitance in interval i, and n_i is the number of samples in that interval. This gives an overall mean that takes into account the size of each interval.

To find how much the values vary within a single interval, we compute the standard deviation as

$$\sigma_i = \sqrt{\frac{1}{n_i} \sum_{j=1}^{n_i} (x_{ij} - \mu_i)^2} \tag{9}$$

where x_{ij} is the j-th capacitance measurement in interval i, μ_i is the average capacitance in that interval, and n_i is again the number of samples.
To measure the overall variation across all intervals, the weighted standard deviation is calculated as

$$\sigma_w = \sqrt{\frac{\sum_i n_i \cdot (\sigma_i^2 + (\mu_i - \mu_w)^2)}{\sum_i n_i}} \tag{10}$$

In this expression, σ_i is the standard deviation of interval i, μ_i is the mean of interval i, μ_w is the overall weighted mean, and n_i is the number of samples in that interval. This formula combines the spread of data within each interval with the spread of the interval means around the global average, giving a complete picture of variation in the entire dataset.

Finally, the coefficient of variation, $V\%$, expresses the weighted standard deviation in relation to the weighted mean is

$$V\% = \left(\frac{\sigma_w}{\mu_w} \right) \cdot 100 \tag{11}$$

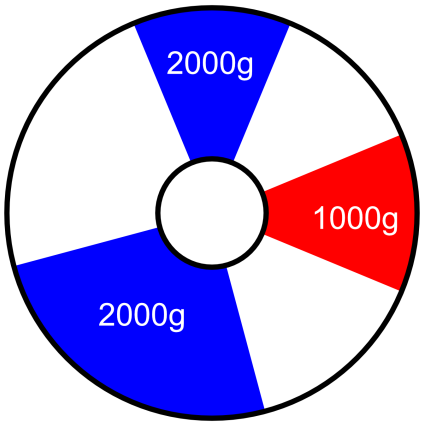

Figure 11: Sample setup for mass testing

Ten LC-tanks was selected with varying sizes and were all tested on each channel and evaluated using the parameters above. From the results, two combinations of LC-tanks were chosen. One pair consisted of the two LC-tank-sizes with the highest resolution for each channel and the other of the sizes with the lowest variation. These pairs were used in all subsequent tests.

2.5.2 Sample Mass

Since the measurement method works by treating the samples as the dielectric of a capacitor, it was deemed necessary to test if the amount of dielectric medium would affect the measurement.

To evaluate the effect of sample weight on the capacitance measurement, tests were conducted using three different samples. The same moisture content (9.00 %) and compactness were maintained for all samples to isolate the effect of mass alone. One sample had the dry weight of 1000 g and the other two 2000 g, which correspond to the standard sample weight and twice as much as in previous tests. The iron ore concentrate was arranged in different ways to discern potential changes due to form and electromagnetic effects. The smaller, 1000 g and one of the larger, 2000 g, samples was spread over a 45° segment of the rotary conveyor, while the other large sample was spread over a 90° segment. Using this arrangement, both the width and the thickness of the samples will be varied. The resulting arrangement can be seen in Figure 11.

2.5.3 Sample Density

Very early tests showed signs of variability, which were hypothesised to stem from varying density of the tested material due to the iron ore concentrates tendency to lump together. This would align with the theoretical understanding of the measuring method, where a less packed material would consist of more air pockets, which in turn would influence the measurements [18]. Therefore, it was deemed necessary to verify how the density of the material affects the measurement.

Three samples with identical moisture content (9.00 %) and dry weight (1000 g) were placed in a PLA-box, described in Section 2.4.3 directly on the conveyor and homogenised. Two of the samples were pressed, one to moderate compaction (250 N) and the other to high compaction (500 N) using the force gauge Sauter FH 500 [19]. Each sample was measured for 30 s over each sensor.

2.5.4 Test Speed

Since conductive materials moving through an electric field create eddy currents, and currents, in turn, generate opposing electric fields, it was deemed necessary to investigate the sample speed and how much it influences the measurement.

To investigate the influence of the rotating acrylic dish's speed on capacitance measurements, the rotational speed was varied from 0.001 revolutions per second (rps) to 0.090 rps.

The program consists of:

- Stationary measurements for each sample
- Two revolutions at 0.001 rps
- Five revolutions at 0.008 rps
- Five revolutions at 0.016 rps
- Five revolutions at 0.090 rps

The program is intended to allow a systematic assessment of the influence of speed on capacitance.

2.5.5 Sample moisture

Once all parameters were accounted for, tests were performed on varying moisture contents to answer the problems defined in Section 1.1.
Initial tests focused on a moisture content range of 8.19 % to 10.55 % to determine whether capacitance measurements could reliably detect an upward trend correlated with increasing moisture. All samples, prepared with a consistent dry weight of 1000 g, were thoroughly stirred to ensure uniform moisture distribution.

To start, testing consisted of stationary tests, where eight samples were equidistantly placed on the conveyor, each being measured for 30 s over each sensor. Continuous tests were also performed according to the program described in Section 2.5.4.

2.5.6 Single Lot Averaging Tests

Due to high uncertainty in the results, a final set of tests was performed, designed to reduce the sources of error. If this sensor were to be implemented on the real conveyor, an average of the capacitance over a large area and time could be used to handle variations. Using the same concept, these tests take the average capacitance of one revolution from 0 to 360° at a speed of 0.015 rps with 5 kg of iron ore concentrate from a single lot spread evenly across the dish.

To ensure that the ore was homogenous for these tests, a sift was 3D-printed with 3 mm wide holes. This eliminated the lumps that form as the ore is mixed, further reducing variance. Another tool was 3D-printed to evenly spread the ore around the dish, making sure the height is similar all around. All single lot averaging tests were performed with 330 pF LC-tanks on both channels due to time limitations.

2.6 Data Analysis

Depending on the type of test, two different methods were used to interpret the data. Mean capacitance was calculated for each sample and documented for later analysis.

2.6.1 Stationary Analysis

For tests where samples were measured while stationary, measurement intervals were selected manually from the plotted data. Attention was given to not counting extremes and abnormal readings that would result in spikes in the data and deviate from the mean capacitance value.

2.6.2 Moving Analysis

In the continuous movement tests, data from the test rig's encoder was used to associate each data point with a specific angle (in degrees). Given that a full rotation is 360°, and the rig contained eight equally spaced sample positions, as mentioned in Section 2.4.3, the rotation was divided into eight segments of 45° each. This segmentation allowed us to estimate the sensor readings corresponding to each sample position. For every 45° interval, the mean capacitance was calculated. This method minimised manual processing but could not detect and exclude anomalies in the recorded data.

3
Results

This chapter will present the results of the tests described in Section 2.5.

3.1 Choice of Measuring Frequency

Table 2: Resolution and variation per LC-Tank configuration for Channel A and B.

LC-tank (pF)	10	20	33	56	75	100	150	220	330
Resolution A (%)	11.3	9.7	14.1	11.0	11.6	7.9	11.3	12.0	12.8
Resolution B (%)	9.4	8.5	9.8	9.6	9.4	8.6	10.4	9.1	8.5
Variation A (%)	0.05	0.06	0.06	0.04	0.04	0.04	0.04	0.02	0.02
Variation B (%)	0.05	0.06	0.06	0.04	0.05	0.04	0.05	0.02	0.01

Among the tested LC-tank configurations, a setup with 33 pF on Channel A and 150 pF on Channel B provided the highest resolution (see Table 2) equivalent to 2.773 MHz and 2.166 MHz for channel A and B respectively.

Additionally, tests indicate that the 330 pF LC-tank exhibits the lowest proportional deviation within the target intervals, meaning 1.712 MHz is optimal for variation, being 0.01 to 0.02 % for both channel A and B.

3.2 Influence From Sample Mass

Table 3: Capacitance given Mass for Different LC-Tanks

Mass (g)	**Capacitance (pF)**			
	33 (pF)	**150** (pF)	**330** (pF)	**330** (pF)
1000 (45°)	165.832	156.553	179.731	161.616
2000 (45°, double height)	167.966	157.765	181.718	162.886
2000 (90°, double width)	166.977	156.879	181.127	162.062

Table 3 illustrates the effect of varying sample weight and spread angle on capacitance measurements. Data shows approximately 2 pF in difference between 1000 g

and 2000 g in dry-weight. The same 2000 g spread over a wider area has less of an impact.

3.3 Influence From Sample Density

Table 4: Capacitance given Compactness for Different LC-tanks

Compactness (N)	**Capacitance (pF)**			
	33 (pF)	**150** (pF)	**330** (pF)	**330** (pF)
0	165.428	156.358	179.396	161.441
250	165.257	156.093	179.246	161.179
500	165.176	156.151	179.178	161.151

Capacitance measurements varied only marginally, 0.2 to 0.3 pF, with compaction force of 0, 250 and 500 N, as shown in Table 4. The capacitance appears to decrease slightly with increasing compactness.

3.4 Influence From Speed

As shown in Figure 12 and 13, the capacitance exhibits a reduction of approximately 0.2 pF with increasing speed. Variations are quite high at each speed, with the median varying by 0.1 to 0.3 pF.

The box plot used to represent these measurements is described as follows:

- **The Box** - Represents the interquartile range (IQR), spanning from the 25th percentile (Q1) to the 75th percentile (Q3) of the measured values. The median (50th percentile) is typically indicated by a line within the box.
- **Whiskers** - Extend to the smallest and largest values within $1.5 \times$ IQR from Q1 and Q3, respectively.
- **Outliers** - Data points outside the whiskers are considered outliers and are displayed as individual points.

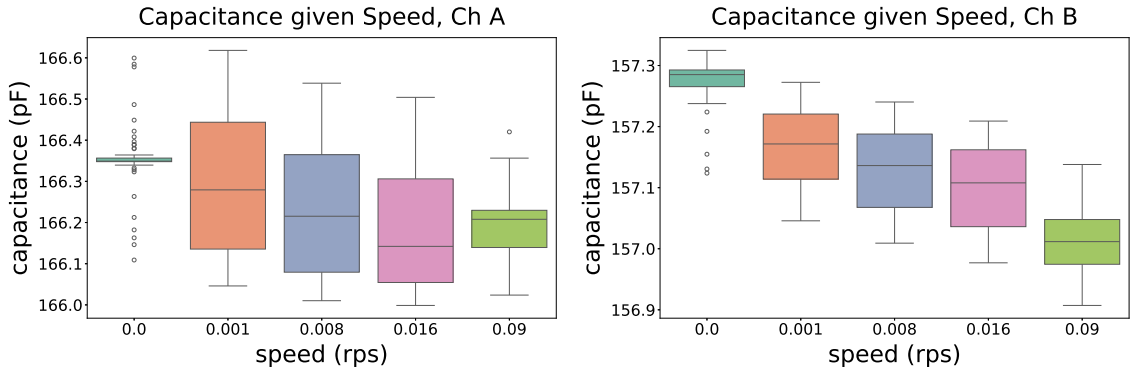

Figure 12: Capacitance given speed, with sample with 9% moisture, 33 pF LC-tank on channel A and 150 pF LC-tank on channel B.

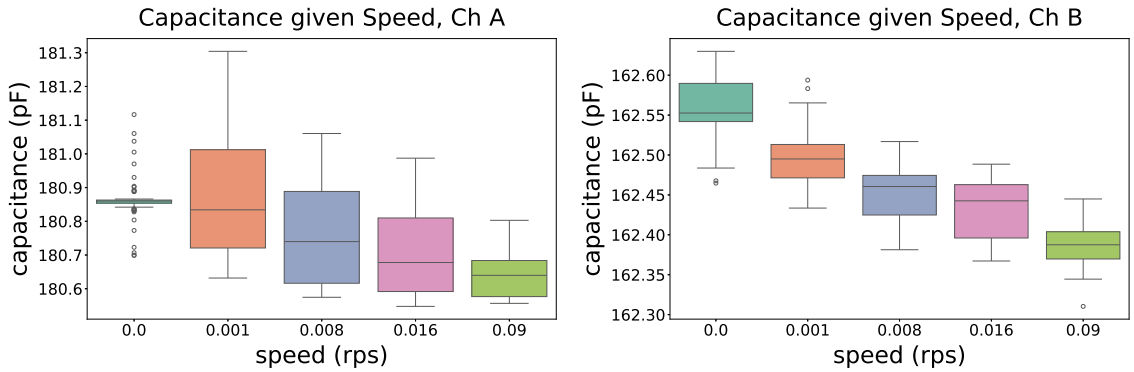

Figure 13: Capacitance given speed, with sample with 9% moisture, 330 pF LC-tanks on both channel A and B.

3.5 Moisture Results

The influence of sample moisture content on capacitance in continuous analysis is detailed in Tables 9 to 12 in Appendix G. Across all experimental runs with both chosen LC-tank configurations, the capacitance range for the moistures studied is between 0.5 and 1.2 pF. The corresponding box plots for the stationary tests are shown in Figure 14. An interesting phenomenon appears at 9.41 % with the 33 pF LC-tank, this is due to the measurement never stabilising, even when stationary. This phenomenon has been encountered in other tests, but the reasons are unclear.

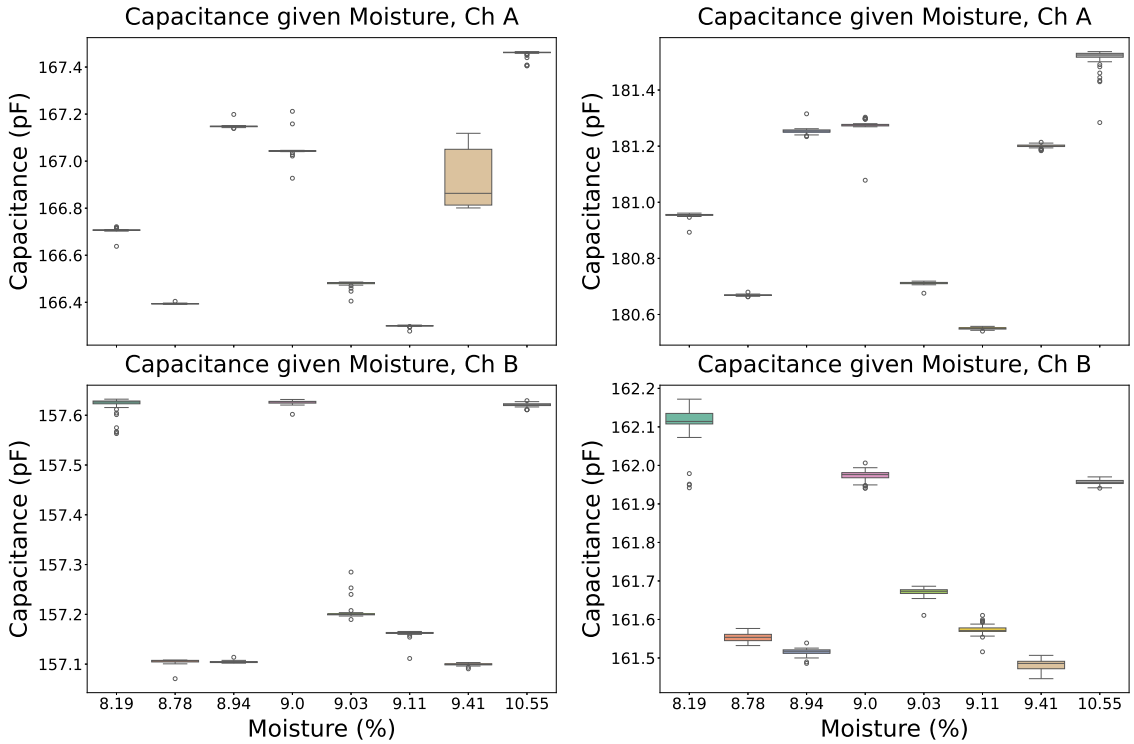

Figure 14: Capacitance given sample moisture content, with 33 pF LC-tank on channel A and 150 pF LC-tank on channel B, aswel as 330 pF LC-tanks on both channel A and B.

3.6 Nugget-To-Sill Ratio

The nugget effect explained in Section 2.3.2 occurred when being tested. Figure 15 below indicate that small errors in moisture content can be observed. The difference in moisture content within the tests are between 0.08 % to 0.12 %. All the tests are done on lot 5 in Table 1.

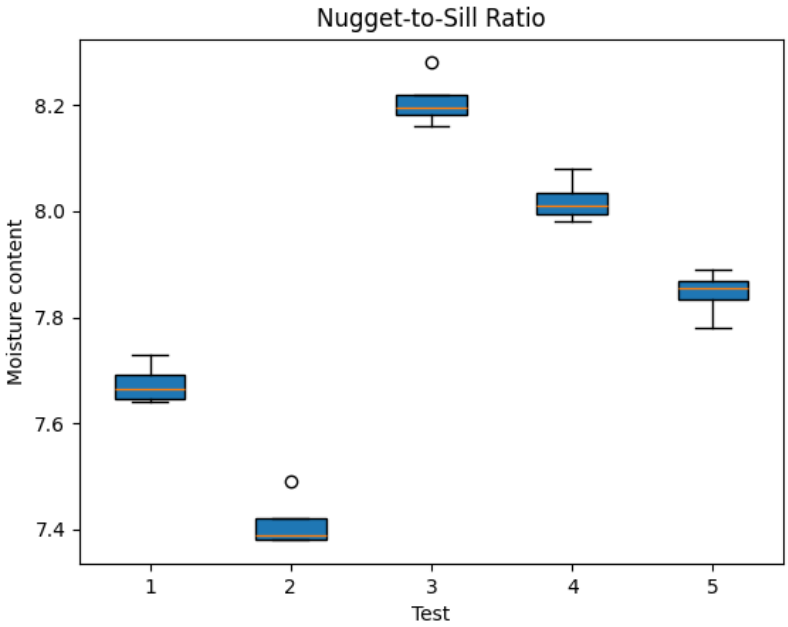

Figure 15: Box-plot illustrating the effect of Nugget-to-Sill ratio from one of the lots.

3.7 Repeatability of Results

Repeatability can be observed in every test, and results have proven to be quite consistent regarding measurements of the same sample at different times.
Figure 16 illustrates the relative consistency of measuring the same samples five times without physically disturbing them. More results from similar tests can be viewed in Appendix G, Table 13 to 16.

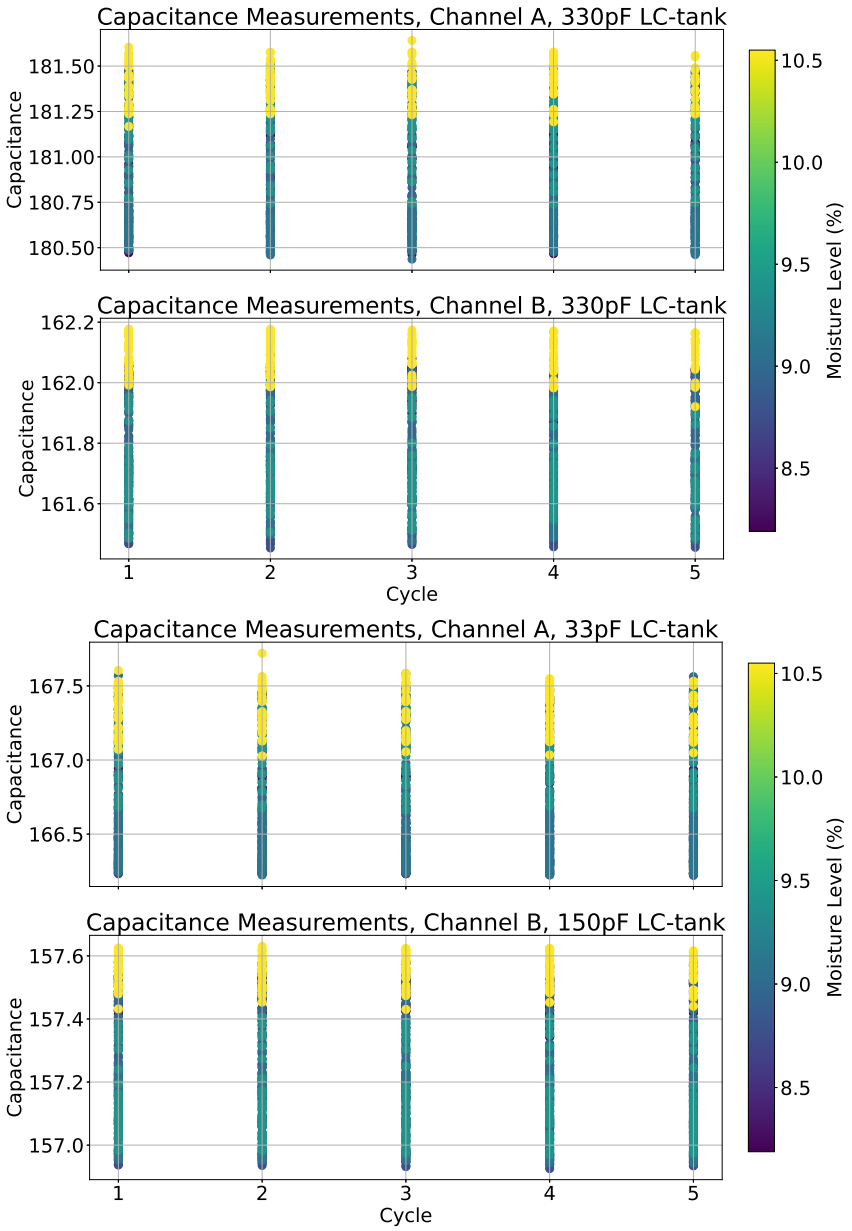

Figure 16: Eight samples measured at five separate times, both with 330 pF LC-tanks on both channels and 33 pF LC-tank on channel A and 150 pF LC-tank on channel B.

3.8 Single Lot Averaging Tests

To confirm that only one rotation is needed for these tests, an initial test was performed on lot 4 with two full rotations. The results of this test are shown in Figure 17 and confirm that the average is similar across rotations.

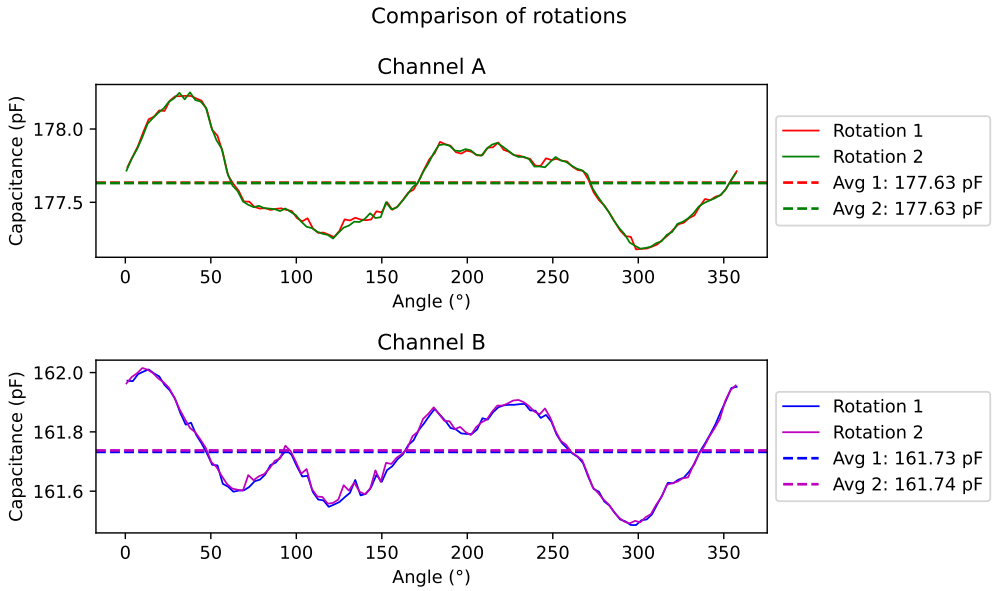

Figure 17: Repeatability test for single lot averaging

Figure 18 shows the average capacitance of lots 1-8 measured with the method described in Section 2.5.6. The tests for lots 1-3 were repeated after lot 8 due to an error in the measurement process.

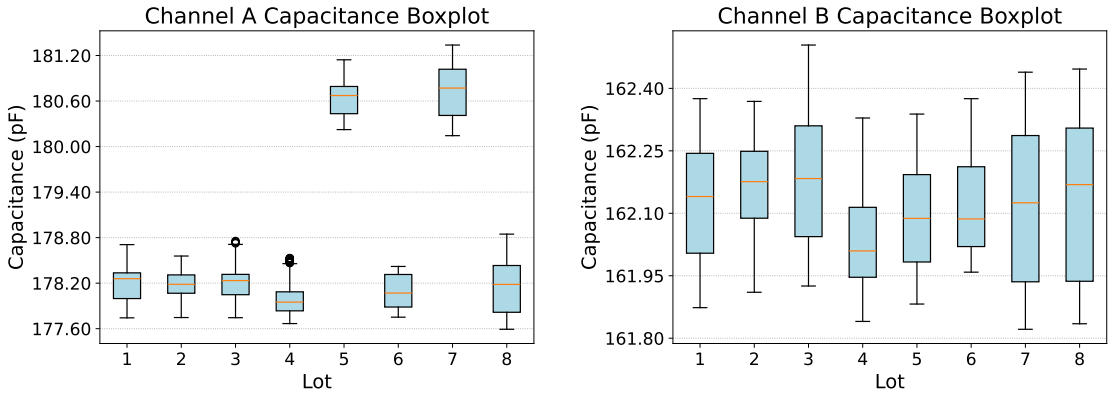

Figure 18: Full conveyor single moisture content tests for lots 1-8

As the tests in Figure 18 indicate inconsistencies in channel A and a sensor drift in channel B, another set of tests was performed. This time, focusing only on channel B and with a constant time between the tests in hopes of getting a constant drift that is possible to filter out. This time, only three lots were tested due to time

limitations, which were lots 7, 5 and 3 in that order. The results for these tests can be seen in Figure 19 and 20.

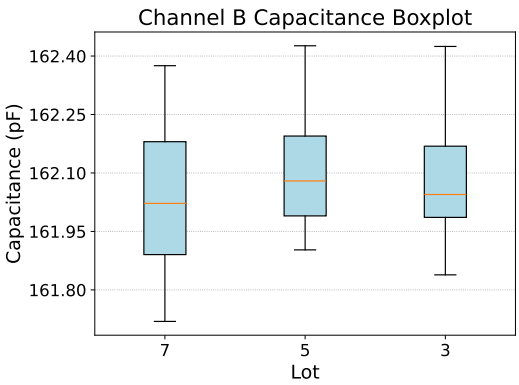

Figure 19: Box plot of second set

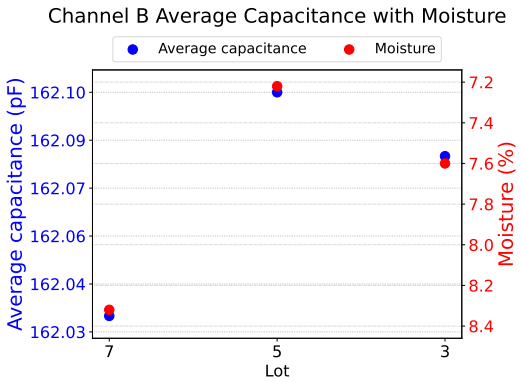

Figure 20: Average capacitance and verified moisture content of the second set

In these tests, drift was not a problem and the data was usable. There also seems to be a clear proportional correlation between the capacitance and verified moisture. To get a formula between capacitance and moisture, linear regression was used on the data. The result of this is shown in Figure 21.

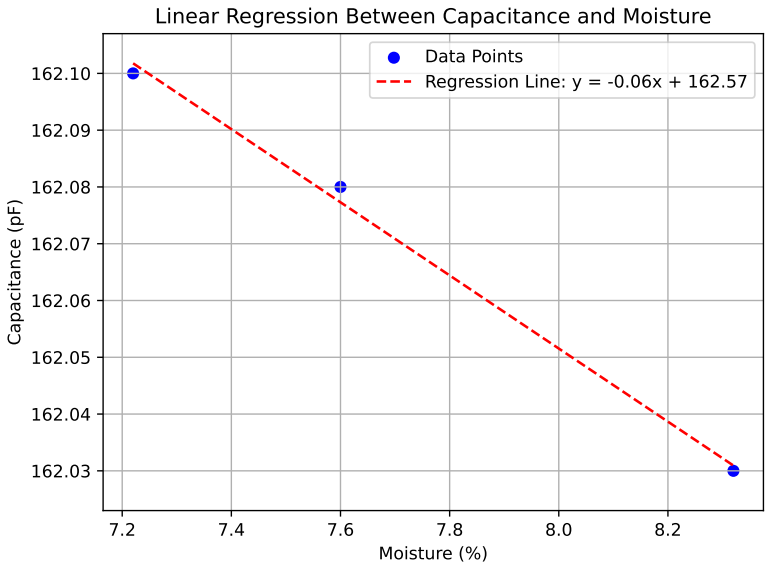

Figure 21: Linear Regression on the Second Set of Tests

If this holds true, the moisture content in the iron ore concentrate can be found using the formula

$$\text{Moisture percentage} = \frac{162.5667 - C \times 10^{12}}{0.0644} \tag{12}$$

where C is the capacitance in F. The R^2 value for this line is 0.9957, which indicates a high accuracy. With only three points though, that does not mean much without further testing.

4
Discussion

Before continuing, it is worth discussing two notable qualities of the data.
First being the varying capacitance ranges in the test results. The test evaluation did account for the LC-tank capacitance, by subtracting it and only reading the capacitance of the conveyor and the iron ore concentrate. Due to manufacturing error margins of the LC-tanks, some of the measured capacitances will vary by approximately 12 pF, this will not affect analysis, since what is of interest is a relative measurement to a calibrated moisture content sample, rather than an absolute measurement.
Secondly, there are flaws in the continuous tests, where at the maximal speed, each sample measured significantly fewer data points, leading to less reliable and sometimes misleading data. The high speed is also hypothesised to slightly move the iron ore concentrate due to centrifugal forces and vibration, which compromises the validity of the results.

4.1 Analysis of Parameter Impact

The measurements suggest that several parameters influence the capacitance of the measured iron ore concentrate and that it may be hard to isolate them in order to decide the moisture content. Below, tests aimed at isolating these parameters will be discussed.

4.1.1 Measuring Frequency Optimization

The differences in measurement resolution certainly is related to the electrode separation, as shown in Figure 3. Additionally, the variation in measurements, notably the minimal proportional deviation of 0.01 to 0.02 % observed in the 330 pF LC-tank configuration indicates high stability across the target intervals, likely due to the higher capacitance reducing sensitivity to external noise.

To further narrow down the selection of measurement frequency, studies on the dielectric behaviour of concentrate could be performed. Given the theoretical understanding that materials display different permittivity under different frequencies, it would be of interest to perform theoretical calculations and analytical measurements to find a more optimised frequency for a given quality of concentrate.

4.1.2 Effect of Mass

As shown in Table 3, the effects of mass seem to be significant. The large samples with a wider spread having a higher capacitance measurement than the baseline sample indicates that there is some kind of electromagnetic effect of a large, continuous sample or the measured field extends further to in the x-y-plane than anticipated. The increase in capacitance from the other sample could be explained by the same hypothesised electromagnetic phenomenon but also a decreased distance to the sensor from deformation of the rotary dish or extension of the measurement field in the z-plane similar to that explained above.

4.1.3 Effect of Material Density

The study found that the density of the material has a small impact on the results as presented in Figure 4. The observed decline in capacitance with higher compactness is contrary to the intuitive reasoning that less air within the material would lead to a higher total permittivity. It is speculated that the reduction could be explained either by more measurements being performed above the measured material or the dielectric properties of the material are altered by higher compactness. Further studies are needed to determine the cause.

4.1.4 Effect of Speed

One trend that became apparent is that the capacitance generally decreases as the speed of the material increases, as shown in Figures 12 and 13. There is, however, an exception at the highest speed shown in Figure 12, with the 33 pF LC-tank, where the capacitance unexpectedly increases. This is explained by the previously mentioned problems encountered when performing the continuous tests.

On the other hand, Figure 12 suggests that the overall variation in measurements is not strongly affected by speed. This could mean that the impact of speed depends on variables like the type of sensor, properties of the material, or the specific capacitance range being measured.

Finally, the edges of the sensor are usually less accurate due to the way the electric field behaves in those areas. When the material moves quickly over these edge zones, the inaccuracies can become more noticeable.

4.1.5 Repeatability of Measurements

The study found that measurements between rotations were essentially identical, indicating high repeatability. This is illustrated in Figures 16 and 17. However, between the different velocities as mentioned in 4.1.4, a similar connection could not be drawn.

In order to implement this system in a real scenario, it is a prerequisite to have repeatability in the results to be able to draw trustworthy conclusions. Therefore, it can be seen as one of the most important discoveries made in this project.

During all tests temperature and humidity have been recorded. The relative humidity was found to be 25.5 to 49.2 % and the temperature 21.3 to 24.4 °C. Any analysis of their effect have not been made, however, the effect of them seems negligible compared to other variations measured.

4.1.6 Effect of Moisture

These readings did not consistently correlate with the moisture content of the concentrate samples, suggesting other factors may influence capacitance measurements. A linear trend is still visible though, especially on channel A.

The variations in moisture of the lot seem to be impacted by the nugget effect, which seems to have an impact on the results. Although steps are taken to homogenise the material, it can not be ensured that the verification sample has the same moisture content as the sample on the test rig. As can be seen in Figure 15, the moisture content can differ more than some levels presented in Table 1, which makes it really hard to determine if the result with certainty can be trusted.

However, the error of moisture variation in the tests may be affected by depurate from the ISO standard described in Section 2.3.2. If bigger samples and several samples from each lot were tested as described in the standard, the validated moisture in the sample would more likely be representative for the whole lot.

An important step in calculating moisture content is to compensate for the parameters influencing on the reading, either with practical methods or by calculations. Given that the parameters have such a high variation and their non-linearity, it proved extremely difficult to create an equation or to model the effect of the parameters accurately.

The initial goal of the project was to test moisture content of 6 to 12 % as presented in Table 1. This was abandoned after realising that the lot with the highest moisture content still had water accumulations present after homogenisation.

4.1.7 Single Lot Averaging Tests

The averaging tests were done as a final effort to find a good correlation between capacitance and moisture by controlling as many variables as possible. The results were promising, but the method could not be explored further as these tests started only days before the project and report had to be finished.

The initial averaging test showed two concerning sources of error that might be

present in other tests performed during this project. Channel A showed inconsistent results, with some tests having a much higher capacitance than the others. Channel B showed strong signs of sensor drift as the average capacitance increased with every test, even after going back to the first lots. Curiously, this sensor drift did not seem to be present in the second set of tests.

The second set of tests showed promising results but would need more data points to confirm that it is not by chance. The resulting linear regression model seems to have a good accuracy but with only three points it is inconclusive. With further testing, including more data points and verifying the model, there is a chance this method could lead to a formula that can correlate capacitance and moisture closely.

With the correlation seeming good in this test, it would seem that sifting the iron ore concentrate through a mesh, and thereby removing most of the lumps, helped give more accurate verification tests as well. If small-scale tests were to continue, this would be a good method to explore further, but it would be even better to go straight to large-scale testing, where many variances caused by the small scale would be avoided.

4.2 FMEA

4.2.1 Rotary Conveyor

Some actions were highlighted as critical in the FMEA. As earlier mentioned, a PID controller was implemented to ensure a precise and constant speed during the tests. To be able to maintain the lowest speed and reach the highest torque required, a gearbox was constructed for the motor. To avoid overloading the motor, a current-limiting power supply was used to drive it. The frame was also reinforced after the first tests to ensure rigidity. All identified failure modes can be seen in Table 6 in Appendix E.

4.2.2 Sensor

According to the FMEA analysis for the sensors, coaxial connectors designed to ensure reliable signal transmission and minimise electrical interference were chosen. This choice was made in order to minimize noise and other disturbances that could significantly affect the measurement results. The electrodes were secured using a 3D-printed casing that held them in place just below the acrylic sheet, maintaining a consistent distance and width to ensure uniform measurement conditions. All identified actions and potential issues have been addressed throughout the project to support accurate and stable measurements, see Table 7 in Appendix E.

4.3 Ethical aspects

This project has been performed in cooperation with LKAB, which has the vision to lead the industry into the future with innovative and competitive solutions. The system developed in this project could result in improvements across several fields. The system could lead to further improvements in pursuit of accomplishing climate goals, especially climate goals 9 and 12 set by the UN, by making the energy consumption more even [20].

4.4 Social aspects

In order to operate basic industry in Europe, especially in Sweden, adaptability and innovative capacity are crucial aspects to compete with industries in other parts of the world with lower production costs. This is essential to keep the industry, jobs and expertise in this part of the world, ensuring human rights and high general standard of living.

The discoveries made in this project would, if implemented, lead to a safer environment for the technicians at the plants. The manual work of taking out a sample for the gravimetric method will be reduced. Calibration to ensure the functionality of the sensors may, however, still be needed.

5
Conclusion

This project set out to answer two main questions:

- What was the feasibility of implementing capacitive iron ore concentrate moisture content measurement in real-time?
- How does the capacitive moisture measurement system compare to traditional methods?

Even though the answer to these questions was not as straightforward as anticipated, the project has come to several conclusions which could provide a foundation for further studies. These conclusions, together with suggestions for areas of further studies, will be provided below.

5.1 Conclusion on Feasibility

During the project, several parameters which has had as large, or larger, impact on the measurement results as change in moisture content have been identified. These include density, distance to sensor, amount of material, and some that are still to be identified. This makes it difficult to answer the question of feasibility accurately. However, the results have shown that there is indeed a measurable difference in capacitance between different moisture contents in the concentrate. It is hypothesised that several of the affecting parameters are the result of small samples and that by measuring larger volumes, many of the local variations will even out and show a more consistent result. Other studies have shown results that are less affected by these parameters, but there is limited research into the effects of relative speed between the sensor and the measured material. This project has shown that the relative speed does not influence the measurements more than what is acceptable. This makes it possible to conclude that it is indeed feasible to develop on-line measurement methods for iron ore concentrate using capacitance, but that the method needs further development using large-scale tests.

5.2 Conclusion Compared to Existing Methods

Due to the issues mentioned above, no real comparative analysis was performed against other, more established methods. The project ran into several problems present in other methods, including sample variability. Tests showed sensor drift, indicating that the method may require periodic calibration, however, further studies may find ways to counteract this. This project is unable to draw any conclusion

regarding the performance of capacitative methods compared to other methods of measuring moisture content of iron ore concentrate.

5.3 Areas for Further Study

To enhance measurement accuracy, sensors should ideally be embedded directly within the iron ore concentrate. Given the abrasive nature of iron ore concentrate, this would most likely not work for a sensor that is supposed to perform measurements in a moving stream of material, but it would still be ideal to try to keep the air gap between sensor and measured material as small as possible. It is therefore suggested that further studies into the subject try designs that would not measure through the conveyor belt. Suggested methods for achieving this are to either mount the sensor to a plough riding on the material, thereby providing a fixed, small distance; a sensor measuring from the side or measuring during free fall in a loading chute.

This project has been exclusively small-scale and even though it has enabled tests with varying moisture contents in a way that would have been difficult to perform in a real production environment, many of the problems encountered most likely stem from the material not behaving the same in small scales. It is therefore recommended that further studies be performed on larger samples, ideally the same size as in a production environment or on-site.

If tests are to be performed on a smaller scale, more emphasis should be put on proper sampling and homogenisation of the tested material since this has been identified as a large source of error, mainly due to the nugget effect caused by uneven moisture distribution in the samples. If a new test rig is to be constructed, it is recommended to leave the circular design for a linear design. Even though the circular conveyor has helped in the ease of repeated tests and material handling, it is not as representative of a real-world implementation. A linear belt design with two opposing directions would require transferring material from one belt to the other, which could provide mixing and thereby certain homogenisation of the material, which could improve results.

To provide a full insight into the methods, areas of further studies include:

- Effects of different minerals, i.e. hematite
- Effects of additives
- Effects of particle size
- Impact from the environment, e.g. temperature and humidity

Bibliography

[1] X.-h. Fan, G.-m. Yang, and X.-l. Chen, "Evaluation model on the ballability of iron ore concentrates," *Powder Technology*, vol. 280, pp. 219–226, 2015. DOI: 10.1016/j.powtec.2015.04.068.

[2] A. Timofeeva, T. Nikitchenko, V. Fedina, and V. Kazartsev, "Effect of the composition and characteristics of the charge materials on the quality of iron-ore pellets," *Metallurgist*, vol. 59, no. 3-4, pp. 212–215, 2015. DOI: 10.1007/s11015-015-0086-5.

[3] SS-ISO 3087:2011, "Iron ores — determination of the moisture content of a lot," International Organization for Standardization, Standard, 2011.

[4] P. Cancilla, P. Barrette, and F. Rosenblum, "On-line moisture determination of ore concentrates 'a review of traditional methods and introduction of a novel solution'," *Minerals Engineering*, vol. 16, no. 2, pp. 151–163, 2003, Solid-liquid separation, ISSN: 0892-6875. DOI: https://doi.org/10.1016/S0892-6875(03)00046-3.

[5] Engström, K.-O. Mickelsson, S. Töyrä, and K. Esbensen, "Improvement of sampling for moisture content analysis in iron ore pellet feed - variographic characterisation and on-line ir-analysis," 2019, pp. 3523–3533.

[6] D. G. Miljak, D. Bennett, T. Kazzaz, and N. G. Cutmore, "On-line microwave moisture measurement of iron ore and mineral concentrates in conveyor applications," in *2006 IEEE Instrumentation and Measurement Technology Conference Proceedings*, (Sorrento, Italy), Apr. 2006, pp. 183–186. DOI: 10.1109/IMTC.2006.328366.

[7] F. Harbert, B. Sjöberg, and J. Bak, "Moisture content measurement in iron ore," *Mining Magazine*, pp. 339–341, Oct. 1973.

[8] G. G. Archer and P. Wang, "The dielectric constant of water and debye-hückel limiting law slopes," *Journal of Physical and Chemical Reference Data*, vol. 19, no. 2, pp. 371–411, 1990. DOI: 10.1063/1.555853.

[9] A. K. Rêgo Segundo, M. J. Da Silva, G. M. Freitas, P. M. De Barros Monteiro, and J. H. Martins, "Reply to comments: A novel low-cost instrumentation system for measuring the water content and apparent electrical conductivity of soils, sensors, 15, 25546–25563," *Sensors*, vol. 18, no. 6, 2018, ISSN: 1424-8220. DOI: 10.3390/s18061742.

[10] M. E. H. Silva, A. K. R. Segundo, S. A. L. d. Silva, and P. M. d. B. Monteiro, "Capacitive, non-invasive and coplanar-electrode transducer for measuring iron ore moisture," *Proceedings*, vol. 42, no. 1, 2020, ISSN: 2504-3900. DOI: 10.3390/ecsa-6-06579.

[11] R. P. Deshpande, "Introduction to capacitors," en, in (Capacitors), 1st Edition, Capacitors. New York: McGraw-Hill Education, 2015, ISBN: 9780071848565.

[12] G. Santos, É. Pinto, A. Silva, P. Monteiro, A. Mesquita, and A. K. Segundo, "Real-time capacitive sensor applied to a train wagon prototype for measuring iron ore moisture," *IEEE Latin America Transactions*, vol. 21, no. 4, pp. 595–601, 2023. DOI: 10.1109/TLA.2023.10128932.

[13] H. A. Radi and J. O. Rasmussen, "Inductance, oscillating circuits, and ac circuits," in *Principles of Physics: For Scientists and Engineers*. Berlin, Heidelberg: Springer Berlin Heidelberg, 2013, pp. 961–998, ISBN: 978-3-642-23026-4. DOI: 10.1007/978-3-642-23026-4_28.

[14] F. Reverter, X. Li, and G. C. M. Meijer, "Stability and accuracy of active shielding for grounded capacitive sensors," *Measurement Science and Technology*, vol. 17, no. 11, pp. 2884–2890, 2006. DOI: 10.1088/0957-0233/17/11/004.

[15] *FDC2x1x Multi-Channel, High Resolution Capacitance-to-Digital Converter for Capacitive Sensing Applications*, 2024. [Online]. Available: https://www.ti.com/lit/gpn/FDC2214.

[16] *KERN EHA 500-2*. [Online]. Available: https://www.kern-sohn.com/cosmoshop/default/pix/a/media/TEHA%20500-2-A/TD_EHA+500-2_en.pdf.

[17] *Kern DE 60K10D*. [Online]. Available: https://www.kern-sohn.com/cosmoshop/default/pix/a/media/DE%2060K10D/TD_DE+60K10D_en.pdf.

[18] B. Clarke, *Microwave Measurements*. The Institution of Engineering and Technology, 2007, ch. 18, pp. 409–458. DOI: 10.1049/PBEL012E_ch18.

[19] *Sauter FH 500*. [Online]. Available: https://www.kern-sohn.com/cosmoshop/default/pix/a/media/TFH%20500-B/TD_FH+500_en.pdf.

[20] Luossavaara-Kiirunavaara AB (LKAB), *Års- och hållbarhetsredovisning 2024*, Luleå, Sverige, 2025. [Online]. Available: https://lkab.com/wp-content/uploads/2025/03/LKAB_2024_Ars-och-hallbarhetsredovisning.pdf.

A

FDC2214 Configuration

Table 5: FDC2214 Configuration

Property	Address	Value
General		
DRDY_2INT	0x19[0:0]	1
WD_ERR2INT	0x19[5:5]	1
AL_WARN2OUT	0x19[11:11]	1
AH_WARN2OUT	0x19[12:12]	1
WD_ERR2OUT	0x19[13:13]	1
INTB_DIS	0x1A[7:7]	0
REF_CLK_SRC	0x1A[9:9]	1
RESERVED	0x1A[10:10]	1
RESERVED	0x1A[12:12]	1
SENSOR_ACTIVATE_SEL	0x1A[11:11]	0
DEGLITCH	0x1B[0:2]	4
HIGH_CURRENT_DRV	0x1B[6:6]	0
RR_SEQUENCE	0x1B[13:14]	0
AUTOSCAN_EN	0x1B[15:15]	1
Channel N		
RCOUNT	0x08+N	32000
SETTLECOUNT	0x10+N	4096
FREF_DIVIDER	(0x14+N)[0:9]	2
FIN_SEL	(0x14+N)[12:13]	1
IDRIVE	(0x1E+N)[11:15]	17

B

Sensor Mount

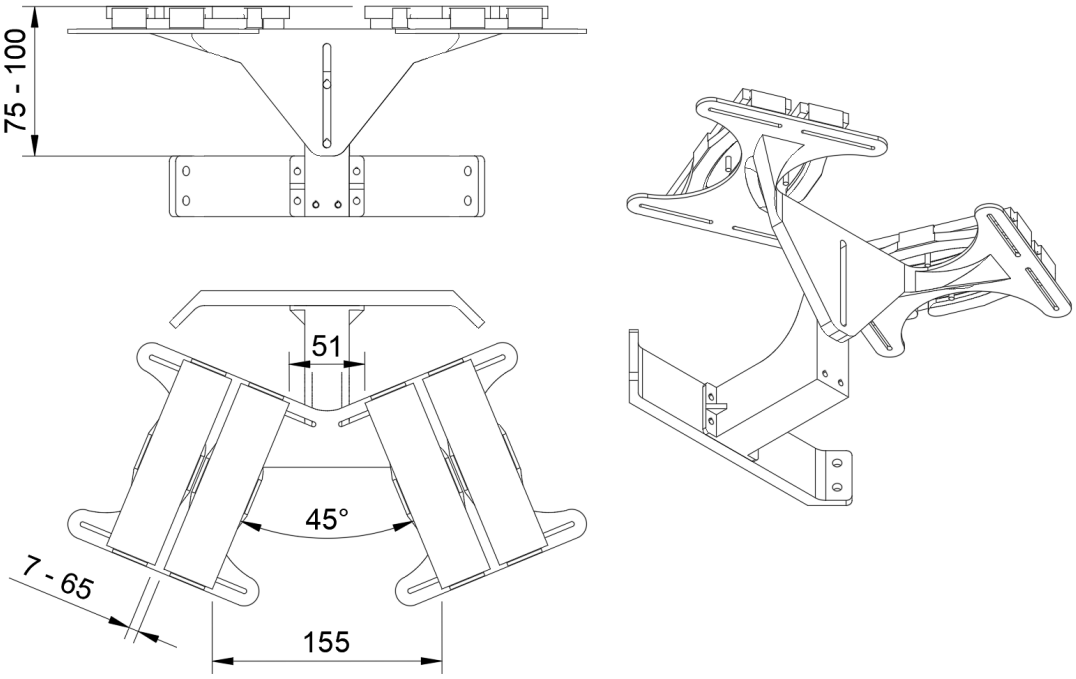

Figure 22: Drawing of Sensor Mount

C

Gearbox Diagram

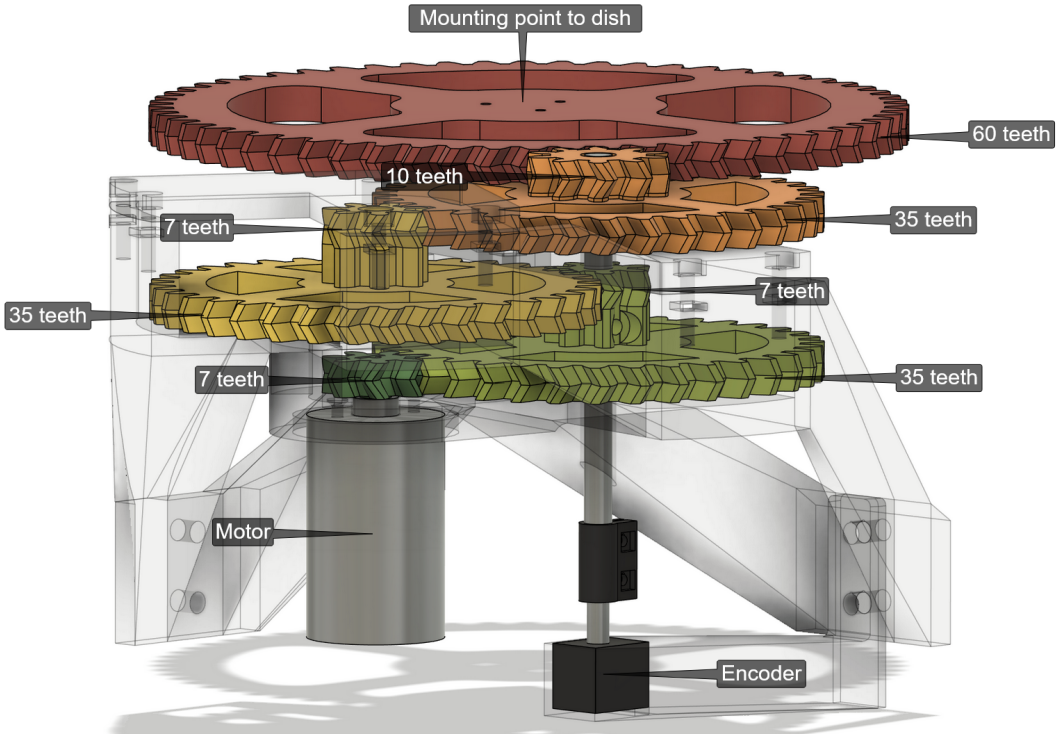

Figure 23: Illustration of the gearbox driving the dish on the test rig. The encoder is connected to the second gear from the motor and the dish is connected to the centre of the last gear.

D

Motor Driver Circuit

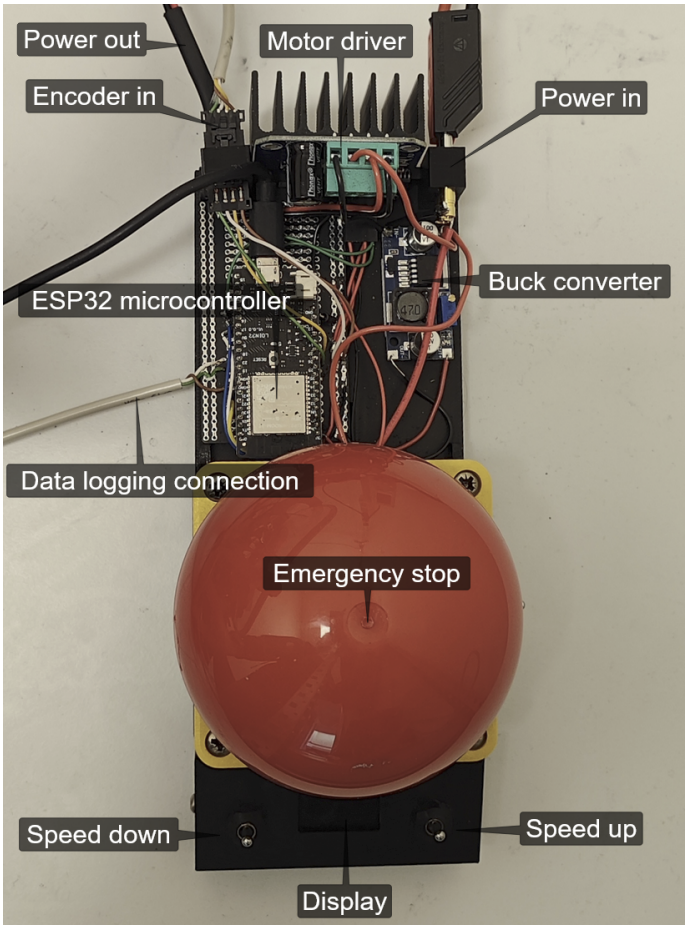

Figure 24: Description of the different parts of the motor driver box.

The motor is controlled by a IBT2 motor driver. The ESP32 microcontroller sets the speed of the motor using pulse width modulation and takes inputs from the buttons. It gives outputs to the display and to the microcontroller logging data from the sensors. The encoder is used as feedback in a PID controller running on the ESP32 that makes sure the speed is correct while the load differs. The parameters for this algorithm are KP = 75000, KI = 50000 and KD = 1000.

E

Failure Mode & Effects Analysis (FMEA)

Table 6: FMEA for Rotary Conveyor

Component	**Failure Mode**	**Cause**	**P**	**E**	**V**	**RPN**	**Action**
Motor	Overloading	Excessive load, incorrect sizing	6	9	7	378	Implement PID controller for precise speed control
Motor	Misalignment	Incorrect installation, wear	5	8	8	320	Use 3D-printed gearbox with precise alignment
Conveyor Belt	Belt Jamming	Blockage due to ore lumps or debris	6	9	8	432	Ensure continuous cleaning
Bearings	Wear and Failure	load distribution, contamination	5	9	7	315	Inspect regularly
Power Supply	Power Loss	Loose connection, overload	6	8	7	336	Use a stabilized power supply and ensure proper connections
Frame/Structure	Vibrations and Instability	Inadequate design, incorrect materials	6	8	8	384	Reinforce the frame

Table 7: FMEA for Sensor and Electronics

Component	**Failure Mode**	**Cause**	**P**	**E**	**V**	**RPN**	**Action**
Sensor plates	Signal deviation	Poor grounding	6	8	8	384	Use shielded cables with grounded copper tape layer to improve grounding.
Sensor plates	Mechanical damage	Wear/tear handling	7	7	9	441	Protective casing, more robust materials
Electronics (PCB)	Overheating	Poor heat dissipation	5	9	7	315	Optimize placement to reduce heat
Electronics (Amp)	Noise/Interference	Poor shielding	6	8	8	384	Use Fakra cables
Power Supply	Power loss	Faulty source/disconnect	5	8	7	280	Improve stability
Microcontroller	Data error	Software bug or faulty ADC reading	4	8	6	192	Debug and validate Arduino MKR Zero code
Wiring	Loose connection	Poor grounding/vibration	5	9	7	315	Secure connections, locking connectors

F

Test Moisture Content

Table 8: Desired Moisture Content Calculation

Function	Expression	Moisture (%)
$f(x)$	1.93^x	-
$b(x)$	$\frac{3f(x)}{f(8)}$	-
x	$9 - b(8)$	6
x	$9 - b(6)$	8.19
x	$9 - b(4)$	8.78
x	$9 - b(2)$	8.94
x	9	9
x	$9 + b(1)$	9.03
x	$9 + b(3)$	9.11
x	$9 + b(5)$	9.41
x	$9 + b(7)$	10.55
x	$9 + b(8)$	12

The formula and calculation used to determine which moisture contents to use to be able to test an error margin down to 0.03%

G
Moisture Cycles

Table 9: 33 pF, Channel A, Capacitance for each Cycle for different Moisture Contents, 0.008 rps

Moisture (%)	**Capacitance (pF)**				
	Cycle 1	**Cycle 2**	**Cycle 3**	**Cycle 4**	**Cycle 5**
8.52	166.430	166.389	166.355	166.377	166.352
8.71	166.085	166.057	166.051	166.051	166.050
9.03	166.104	166.083	166.080	166.072	166.073
9.11	166.536	166.518	166.499	166.511	166.490
9.11	166.095	166.075	166.078	166.069	166.083
9.22	166.616	166.581	166.559	166.557	166.557
9.41	166.594	166.666	166.670	166.658	166.662
10.55	167.095	167.080	167.079	167.065	167.075

Table 10: 150pF, Channel B, Capacitance for each Cycle for different Moisture content

Moisture (%)	**Capacitance (pF)**				
	Cycle 1	**Cycle 2**	**Cycle 3**	**Cycle 4**	**Cycle 5**
8.52	157.381	157.348	157.343	157.344	157.339
8.71	156.924	156.894	156.885	156.892	156.879
9.03	156.919	156.899	156.903	156.896	156.890
9.11	156.777	156.763	156.760	156.762	156.754
9.11	156.923	156.905	156.902	156.904	156.894
9.22	157.193	157.174	157.170	157.173	157.163
9.41	156.917	156.914	156.920	156.913	156.913
10.55	157.234	157.224	157.224	157.219	157.215

Table 11: Channel A, 330pF, Capacitance for each Cycle for different Moisture content, 0.008 rps

Moisture (%)	**Capacitance (pF)**				
	Cycle 1	**Cycle 2**	**Cycle 3**	**Cycle 4**	**Cycle 5**
8.52	180.576	180.515	180.531	180.512	180.523
8.71	180.323	180.303	180.291	180.296	180.285
9.03	180.280	180.264	180.260	180.260	180.245
9.11	180.676	180.664	180.659	180.648	180.645
9.11	180.282	180.275	180.264	180.265	180.255
9.22	180.707	180.675	180.661	180.659	180.644
9.41	180.669	180.731	180.720	180.720	180.714
10.55	181.105	181.112	181.097	181.097	181.081

Table 12: Channel B, 330pF, Capacitance for each Cycle for different Moisture content, 0.008 rps

Moisture (%)	**Capacitance (pF)**				
	Cycle 1	**Cycle 2**	**Cycle 3**	**Cycle 4**	**Cycle 5**
8.52	162.434	162.437	162.426	162.429	162.421
8.71	161.974	161.979	161.966	161.972	161.957
9.03	161.977	161.978	161.973	161.969	161.963
9.11	161.878	161.986	161.869	161.983	161.868
9.22	162.242	162.230	162.234	162.224	162.224
9.41	162.016	162.008	162.010	162.000	162.001
10.55	162.300	162.295	162.295	162.286	162.294

Table 13: Capacitance Measurements for different speeds, 2 cycles, 33 pF. Channel A. Sorted by Moisture (%) within each cycle.

0.001 rps		0.016 rps	
Moisture (%)	Capacitance (pF)	Moisture (%)	Capacitance (pF)
Cycle 1			
8.52	166.521	8.52	166.371
8.71	166.151	8.71	166.049
9.03	166.227	9.03	166.069
9.11	166.166	9.11	166.068
9.11	166.592	9.11	166.498
9.22	166.858	9.22	166.549
9.41	166.954	9.41	166.612
10.55	167.240	10.55	167.043
Cycle 2			
8.52	166.474	8.52	166.320
8.71	166.130	8.71	166.061
9.03	166.161	9.03	166.054
9.11	166.146	9.11	166.077
9.11	166.600	9.11	166.540
9.22	166.697	9.22	166.495
9.41	166.736	9.41	166.657
10.55	167.158	10.55	167.055

Table 14: Capacitance Measurements for different speeds, 2 cycles, 150 pF. Channel B. Sorted by Moisture (%) within each cycle.

0.001 rps		0.016 rps	
Moisture (%)	Capacitance (pF)	Moisture (%)	Capacitance (pF)
Cycle 1			
8.52	157.523	8.52	157.334
8.71	156.955	8.71	156.882
9.03	156.947	9.03	156.884
9.11	157.002	9.11	156.891
9.11	156.805	9.11	156.754
9.22	157.340	9.22	157.157
9.41	156.950	9.41	156.902
10.55	157.348	10.55	157.213
Cycle 2			
8.52	157.412	8.52	157.316
8.71	156.956	8.71	156.852
9.03	156.964	9.03	156.871
9.11	156.953	9.11	156.879
9.11	156.817	9.11	156.761
9.22	157.242	9.22	157.145
9.41	156.953	9.41	156.912
10.55	157.268	10.55	157.208

Table 15: Capacitance Measurements for different speeds, 2 cycles, 330 pF. Channel A. Sorted by Moisture (%) within each cycle.

0.001 rps		0.016 rps	
Moisture (%)	Capacitance (pF)	Moisture (%)	Capacitance (pF)
Cycle 1			
8.52	180.696	8.52	180.495
8.71	180.410	8.71	180.290
9.03	180.400	9.03	180.253
9.11	180.352	9.11	180.260
9.11	180.732	9.11	180.641
9.22	180.894	9.22	180.645
9.41	180.866	9.41	180.716
10.55	181.191	10.55	181.077
Cycle 2			
8.52	180.612	8.52	180.468
8.71	180.357	8.71	180.289
9.03	180.321	9.03	180.248
9.11	180.315	9.11	180.274
9.11	180.719	9.11	180.658
9.22	180.749	9.22	180.628
9.41	180.765	9.41	180.739
10.55	181.155	10.55	181.075

Table 16: Capacitance Measurements for different speeds, 2 cycles, 330 pF. Channel B. Sorted by Moisture (%) within each cycle.

0.001 rps		0.016 rps	
Moisture (%)	Capacitance (pF)	Moisture (%)	Capacitance (pF)
Cycle 1			
8.52	162.512	8.52	162.416
8.71	162.051	8.71	161.945
9.03	162.034	9.03	161.951
9.11	162.034	9.11	161.966
9.11	161.925	9.11	161.865
9.22	162.299	9.22	162.216
9.41	162.045	9.41	162.018
10.55	162.329	10.55	162.295
Cycle 2			
8.52	162.474	8.52	162.412
8.71	162.016	8.71	161.944
9.03	162.001	9.03	161.951
9.11	162.001	9.11	161.959
9.11	161.888	9.11	161.870
9.22	162.259	9.22	162.215
9.41	162.014	9.41	162.008
10.55	162.306	10.55	162.288

DEPARTMENT OF SOME SUBJECT OR TECHNOLOGY
CHALMERS UNIVERSITY OF TECHNOLOGY
Gothenburg, Sweden
www.chalmers.se

CHALMERS